COMPARISON OF SIMULATED HEAT AFFECTED ZONE MICROSTRUCTURES OF NIOBIUM MICROALLOYED STEELS SUBJECTED TO MULTI-PASS WELD THERMAL CYCLES

T. Lolla[1], S. S. Babu[1], S. Lalam[2], M. Manohar[2]

[1]Department of Materials Science and Engineering
The Ohio State University, Columbus, Ohio – 43221
[2]Arcelor-Mittal Global R&D, East Chicago, Indiana 46312

Keywords: Intercritically Reheated Heat Affected Zone, Multi-pass Weld, Characterization, Dilatometry, MA Constituents, Hardness

Abstract

A weldable material's system design includes optimization of base metal (BM), heat-affected-zone (HAZ) and weld metal (WM) microstructure, for a given welding process condition, to achieve target mechanical properties. Traditional research focused on single-pass weld thermal cycles with different HAZ peak temperatures and mostly ignored the effect of initial microstructure. In this research, weldable materials system design methodology is applied to thick plate steels (up to 25 mm) made with niobium microalloying additions. The overarching goal of this research is to optimize the HAZ microstructure evolution to minimize the degradation of properties achieved by original thermomechanical processing, irrespective of the number of weld passes.

Two niobium microalloyed steels with different initial microstructures were studied. The samples were subjected to simulated multipass weld HAZ thermal cycles typically utilised in linepipe production using a Gleeble thermomechanical simulator. Concurrent dilatometric measurements provided insight into phase transformation kinetics. Two sets of experiments were performed and the samples were characterized with optical and scanning electron microscopy, electron back scattered diffraction and microhardness testing.

In the first experiment, for a given composition, samples with different initial microstructures (ferrite + pearlite or bainite + martensite) but the same initial composition were subjected to two pass thermal cycles. In both cases, the final microstructures in these two samples were found to be a mixture of ferrite and small fractions of martensite-austenite (MA) constituents. However, differences in MA content were observed.

In the second experiment, steels with different initial microstructure and different compositions were subjected to multipass weld thermal cycles with peak temperatures above and below Ac_1 and Ac_3 temperatures. These thermal cycles are similar to those expected during multi-pass welding of a thick plate. Interestingly, the final microstructure was found to be invariant (polygonal ferrite) in both the samples. The differences in hardness between these samples were found to be small. This demonstrates that the effect of initial microstructure attained during original thermo-mechanical processing is minimal on the intercritical HAZ in multipass welds.

Introduction

During steel making, alloying (Mo, Nb, V, Si, Cr, Ni, Cu and Mn) and thermo-mechanical processing conditions are optimized to achieve a microstructure that yields a good combination of properties, primarily strength and toughness. Addition of microalloying elements including Mo, Nb and V, control the austenite recovery, recrystallization and grain growth, while the addition of Si, Mn, Ni and Cr modifies the austenite to ferrite phase transformation kinetics [1]. In certain steels, Cu is intentionally added to provide solid solution and precipitation strengthening. For in-service applications of these steels, welding is a necessary final fabrication step. However, weld thermal cycles will alter the carefully engineered initial microstructure of these steels and potentially adversely affect the strength and toughness in the heat-affected-zone (HAZ). In a single-pass weld, the region of lowest toughness is expected to be the coarse grain heat-affected-zone (CGHAZ) [2], the region immediately adjacent to the weld fusion line. In this region, the steel gets heated to temperatures close to melting (typically > 1300 °C), and well above the Ac_3 temperature. This high temperature leads to dissolution of precipitates [e.g. Nb(CN)] which in turn promotes the growth of austenite grains in this region. On cooling from this temperature, brittle microstructures (typically martensite during rapid cooling and upper bainite during slow cooling) may form in this region. The impact of this brittle microstructure in the CGHAZ has been studied extensively in the past [3], however, welding of structural steels often requires multiple weld passes and hence, it is important to understand material HAZ properties when subjected to such multiple weld thermal cycles as opposed to just a single-pass weld.

A multi-pass weld thermal cycle causes the reheating of the initial HAZ, primarily the CGHAZ during subsequent passes, and the final microstructure depends on the peak temperature attained during the subsequent passes (above Ac_3; between Ac_1 and Ac_3; or below Ac_1 or combinations thereof). This new HAZ is again classified into super-critically reheated HAZ (SCRHAZ), inter-critically reheated HAZ (ICRHAZ) and sub-critically reheated HAZ (SRHAZ) respectively [4]. Among these, ICRHAZ has received considerable attention over past years because of the low toughness properties of the microstructure in this region [4, 5, 6]. Interestingly, the toughness of a single-pass CGHAZ microstructure was found to be higher than that of ICRHAZ microstructure [4, 6, 7]. For example, the Charpy toughness of CGHAZ was 360 J at -10 °C and for ICRHAZ was 25 J at -10 °C [4] in a 0.13 wt% carbon steel. This low toughness in the ICRHAZ region is believed to be due to the formation of local brittle martensite-austenite (MA) constituent microstructures [3, 4, 6, 8]. MA constituents form during the inter-critical weld thermal cycle when the austenite islands nucleated at the prior-austenite grain boundaries and bainite lath boundaries [6, 8, 9] are enriched with carbon. This carbon enrichment could cause the austenite to stabilize at room temperature and could lead to local brittle zones [4, 10]. For this reason, it is important to understand the formation of MA constituents during multi-pass weld thermal cycles and its effect on the properties of the material.

Over the past years, the poor toughness of ICRHAZ has been discussed with respect to the formation of MA constituents. For example, Kim et al [4] have evaluated the fracture transition temperature from Charpy impact testing as a function of volume fraction of MA constituents. In this study, the Charpy toughness decreased with an increase in volume fraction of MA constituents. Davis et al [9] studied the importance of cooling rate in the ICRHAZ and its effect on the toughness of steels. It was shown that the faster cooling time (5 s) from the intercritical temperature resulted in a significant lowering of toughness (100 J) compared to that observed for

a slower cooling time (200 s; 300 J). Furthermore, the role of blocky MA constituents on the cleavage initiation in materials with varying MA constituents [6] was studied. It was found that the presence of blocky MA constituents around the grain boundaries contributed towards toughness reduction. Some researchers have also studied the effect of various alloying elements on the formation of MA constituents, for example, the effect of vanadium and niobium on ICRHAZ properties by the formation of MA constituents [3, 9, 11], the effect of silicon on formation of MA constituents in ICRHAZ [12] etc. Additionally, studies have also been conducted to understand the effect of the MA morphology on ICRHAZ properties [12] and the mechanism of brittle fracture in ICRHAZ [6, 13, 14]. However, no work has been reported in the literature related to the effect of initial microstructure on the formation of MA constituents during multi-pass welding of niobium microalloyed steels.

In this work, the role of initial microstructure on the formation of MA constituents is investigated during a multi-pass weld thermal cycle. For this study, steels with the same composition but with different initial microstructures are subjected to a two-pass weld thermal treatment so as to simulate an ICRHAZ microstructure. The amount of MA constituents formed in these steels is quantified using image analysis and the results are presented. In addition, two steels with different compositions and differing initial microstructures are subjected to a multi-pass weld treatment and the resultant differences between the microstructures are examined using microhardness testing.

Starting Materials and Microstructure

Two steels are considered in this study and the compositions of the steels (designated Steel A and Steel B) are given in Table I. The steels differ only in the C, Mn and Si alloying additions and have the same amount of microalloying additions (Ti, V and Nb). Both the steels were thermo-mechanically controlled rolled to a final thickness of 1 inch. The steels were sectioned perpendicular to the rolling direction and samples were taken from the middle of these cross sections. These samples were mounted and polished to < 1 µm using standard polishing techniques and etched using 5% Nital. The steel microstructures were characterized using optical microscopy and hardness measurements. The results of the characterization are discussed below.

Table I. Compositions of Nb Microalloyed Steel A and Steel B wt%

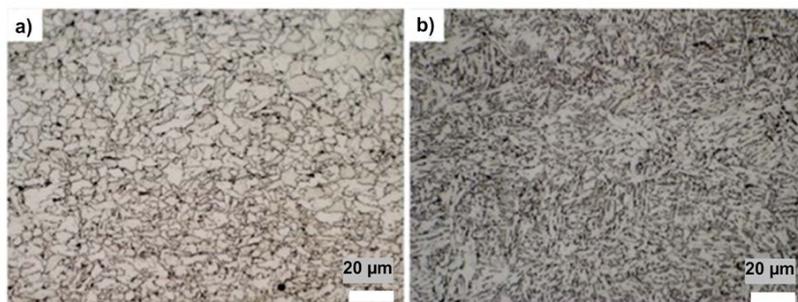| Composition	C	Mn	Si	Cr	Mo	Nb	Ti	V
Steel A	0.04	1.49	0.203	0.02	0.146	0.082	0.019	0.003
Steel B	0.08	1.8	0.45	0.02	0.146	0.082	0.019	0.003

Figure 1. (a) As-rolled microstructure of Steel A showing polygonal ferrite microstructure, (b) As-rolled microstructure of Steel B showing Acicular/Widmanstätten type grains.

The initial microstructures of the two steels are shown in the Figures 1(a) and 1(b). The optical microstructure of Steel A shows predominantly fine polygonal ferrite grains with grain sizes ranging from 6~9 µm, Figure 1(a). The presence of acicular/Widmanstätten type microstructure was also observed at localized regions from the optical images. No significant variation in microstructure was seen along the thickness of the sample. In comparison, the microstructure of Steel B, Figure 1(b), consisted of a fine acicular/Widmanstätten microstructure indicated by the presence of a fine lath morphology. Microhardness indents were made on the cross-section of the samples using a load of 300 g and the average value of hardness for steel A was found to be 212 ± 7 HV whereas, the average microhardness of Steel B was found to be 240 ± 17 HV. In order to study the effect of initial microstructure on MA constituents formed in the ICRHAZ, only Steel A is considered. For this purpose, samples extracted from Steel A were heat treated in order to obtain another different initial microstructure as explained below.

Heat Treatment To Generate Different Initial Microstructure

In order to study the effect of initial microstructure, it is essential to maintain the composition of the steel constant. For this reason, some samples taken from Steel A were subjected to a heat treatment to generate another initial microstructure. This would then produce two sample sets from Steel A, each having a different initial microstructure. This heat treatment was performed on a Gleeble® thermo-mechanical simulator. The samples machined from Steel A were in the form of cylindrical rods with a diameter of 6.35 mm. The thermal cycle and microstructure of the steel thus obtained are discussed below.
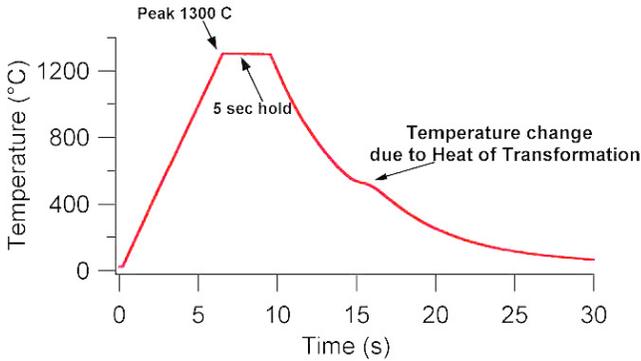
Figure 2. Temperature vs. time graph showing thermal cycle used for obtaining a bainitic/martensitic microstructure in Steel A.

Figure 2 shows the thermal cycle used to generate a different initial microstructure in Steel A. The steel was rapidly heated to a peak temperature of 1300 °C, held for 5 seconds at the peak temperature and finally allowed to cool between water-cooled copper jaws. The free span length between the copper jaws was 10 mm. The cooling rate between 800 and 500 °C ($t_{8/5}$) was found to be ~80 °C/s. The whole heat treatment was carried out in an argon atmosphere. After the heat treatment, the cylindrical sample was sectioned in the region of heat treatment and polished to ~1 μm. From the CCT diagram of Steel A, Figure 3 with a superimposed cooling curve, generated from JMatPro®, the above cooling rate of the steel would lead to a mixed microstructure of bainite and martensite along with a small fraction of ferrite. Figure 4 shows the microstructure generated from this heat treatment. The microstructure in the optical image consists of a mixture of bainite and martensite, as expected from the CCT diagram. Steel A with martensite + bainite as the initial microstructure is referred to as Steel *A1*, Table II. Steel A and Steel *A1* are subjected to a two-pass weld HAZ treatment as discussed in the next section.
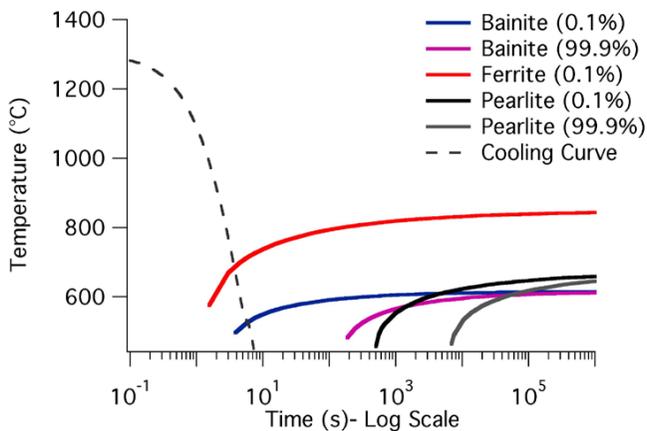
Figure 3. CCT diagram for Steel A generated from JMatPro®, predicting the formation of a mixed bainitic + martensitic microstructure along with some ferrite when subjected to a thermal cycle shown in Figure 2.

Figure 4. Microstructure of Steel A after the heat treatment (Figure 2); Steel A with this microstructure is now referred to as Steel *A1*.

Table II. The Composition and Microstructure of the Three Steels Studied in this Work

Name	Composition (See Table I)	Microstructure
Steel A	Steel A	Polygonal Ferrite
Steel B	Steel B	Widmanstatten/Acicular Ferrite
Steel *A1*	Steel A	Bainite + Martensite

Experimental

Gleeble Simulations for ICRHAZ Microstructure

In order to generate an ICRHAZ microstructure, a two pass weld HAZ thermal cycle was simulated using Steel A and Steel *A1*. For this simulation, a Gleeble® thermo-mechanical simulator was used and the experiments were performed in an argon atmosphere. 'C' type thermocouples were welded to the center of the Gleeble samples to monitor the temperature changes during the treatment. A transducer was attached to monitor the phase transformations occurring during the thermal cycle. The welding cycle parameters used for the HAZ simulation thermal cycle are given in Table III. Figure 5 shows the thermal cycle used in the HAZ simulation for the generation of the ICRHAZ. The details regarding the thermal cycle are provided below.
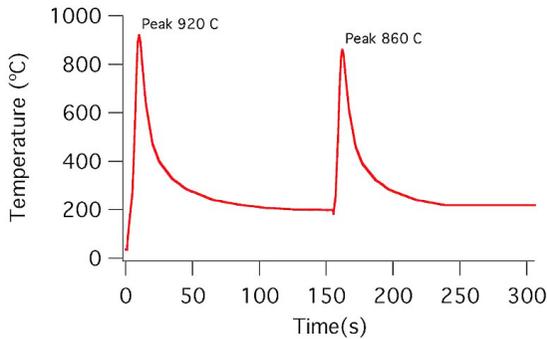

Figure 5. Thermal cycle for the generation of ICRHAZ microstructures in Steel A and Steel *A1.*

Table III. Welding Parameters and Number of Welding Passes used for Simulation

Current (A)	Voltage (V)	Travel Speed - cm/s (ipm)	Heat input - kJ/cm (kJ/in)	Number of Passes
400	35.0	0.76 (18.0)	18 (46.7)	2

As shown in Figure 5, for the first weld pass a peak temperature of 920 °C was chosen. At this temperature, the steel is in the completely austenitic regime as can be seen from the dilatometric results discussed later. The heating rate to the first peak was ~169 °C/s and the cooling time, $t_{8/5}$ was ~44 s. For the second weld pass, the peak HAZ temperature was chosen to be 860 °C which lies between the Ac_1 and Ac_3 temperatures of Steel A (see dilatometry results in next section). The heating rate for the second cycle was ~150 °C/s and the $t_{8/5}$ was ~42 s. The cooling cycle for both the peaks was governed by a Rosenthal-type cooling curve. Samples from both Steel A and Steel *A1* were subjected to the above thermal cycle and the heat treated samples were sectioned

and the microstructure was characterized using optical and scanning electron microscopy and the amount of MA constituents was quantified using image analysis techniques.

Simulations of Multi-Pass (>2) Weld HAZ Thermal Cycle

In order to compare and evaluate the effect of welding on the HAZ microstructure of Steel A and Steel B, a simulated multi-pass welding heat treatment test was conducted. A 16 weld pass HAZ simulation was performed on Steel A and Steel B samples to understand and compare the effect of a large number of weld passes on the HAZ of these two Nb microalloyed steels as explained below. In order to determine the peak temperatures reached during each welding pass at a region adjacent to the fusion boundary, i.e. in the CGHAZ, a finite element heat transfer simulation was used. The joint geometry, welding parameters for the simulation and the description of the experimental setup for the Gleeble tests are explained below.

Finite Element Modeling. For the heat transfer simulation of a multi-pass submerged arc weld, a 2-D FEA welding simulation program called EWI-WeldPredictor® [15] was used. A single bevel groove joint geometry was simulated with a root gap of 1.27 cm (0.5 in), bevel angle of 15° and a root face of 0.317 cm (0.125 in). The welding parameters used for the simulation are the same as in Table III. From the simulation, peak temperatures attained per welding pass were recorded at a point in the HAZ located at half the thickness of the steel. These peak temperatures are used for the Gleeble simulations. For the cooling cycle between successive passes, a Rosenthal type cooling was used similar to the case of two-pass weld HAZ thermal cycle. Figure 6 shows the generated thermal cycle from the data obtained from the FEA simulation. It can be seen from the thermal cycle that three of the welding passes heat the HAZ to temperatures above the Ac_3 temperature (two over 1250 °C and one over 1000 °C). Using this information generated, thermal cycle Gleeble thermal simulations were performed.
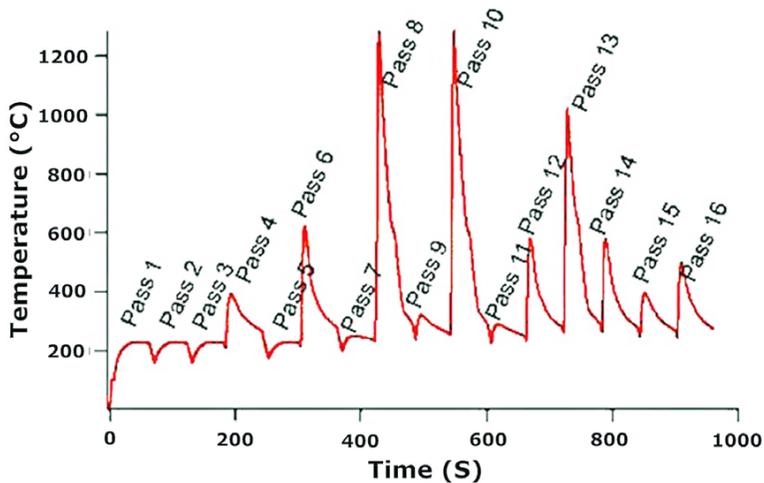
Figure 6. Generated thermal cycle for multi pass HAZ using an FEA model for peak temperature and Rosenthal-type cooling curves.

Gleeble Simulations. Both Steel A and Steel B were subjected to the above generated thermal cycle, Figure 6. To record any phase transformation events occurring during the treatment, dilatometric measurements were also made. The samples were characterized following the same procedure as explained earlier. To compare the mechanical heterogeneity in the HAZ region of Steel A and Steel B, microhardness indents were made on the cross section of the samples. The results obtained from the two-pass weld ICRHAZ simulation between Steel A and Steel *A1* and the multi-pass weld ICRHAZ simulation between Steel A and Steel B are discussed in the next section.

Results and Discussions

Analysis of ICRHAZ Microstructure

Dilatometry Analysis. In this section, dilatometric analysis of phase transformations occurring during the two-pass weld HAZ simulation on Steel A and Steel *A1* is presented. Figure 7(a) and 7(b) are the overall heat treatment graphs showing the relative dilatations of Steel A and Steel *A1* respectively, with respect to the temperature of the two-pass weld HAZ simulation. It can be seen from the graphs that for a peak temperature of 920 °C (during the first heating cycle), the steels undergo complete ferrite to austenite transformation (i.e. above Ac_3). This region would then represent a fine grain heat-affected zone (FGHAZ) developed in the HAZ during single pass welding. In the FGHAZ, the steel temperature rises to just above the Ac_3 temperature but does not undergo grain coarsening as severely as seen in CGHAZ [2]. Using such curves generated by

dilatometry during treatment of Steel A and Steel *A1*, the transformation start and finish temperatures occurring during each peak of the simulation were captured and analyzed.

From dilatometric analysis of the heating regime during the first pass of Steel A, the Ac_1 temperature of Steel A was found to be 764 ± 4 °C and the Ac_3 temperature was 906 ± 6 °C. In comparison, Ac_1 and Ac_3 temperatures for Steel *A1* were found to be 797 ± 4 °C and 902 ± 5 °C. Similar analysis was performed on the cooling part of the curves for both Steel A and Steel *A1*. The results are shown in Table IV.
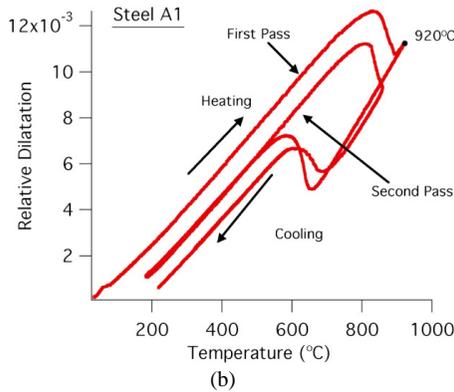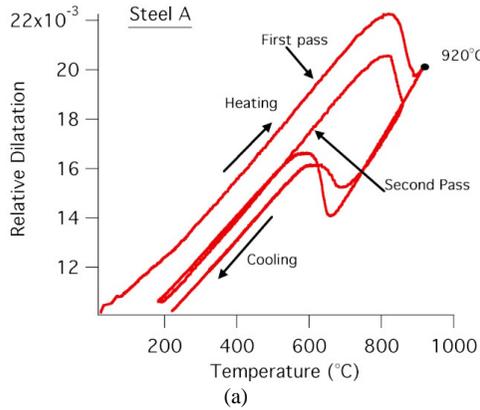

Figure 7. Dilatometry with reference to temperature of (a) Steel A and (b) Steel *A1* for the two-pass weld HAZ treatment showing complete austenitization after 1st pass ($> Ac_3$) and incomplete austenitization ($Ac_1 < 860$ °C $< Ac_3$) in second pass.

Table IV. Comparison of On-Heating (Ac_1 and Ac_3) and On-Cooling (Ar_1 and Ar_3) Transformations for Steel A and Steel *A1* during First and Second Weld Pass HAZ Thermal Cycle

	On-Heating	On-Cooling	
	First Pass (°C)	First Pass (°C)	Second Pass (°C)
Steel A	$Ac_1= 764$	$Ar_1=557$	$Ar_1=572$
	$Ac_3= 906$	$Ar_3=691$	$Ar_3=725$
Steel *A1*	$Ac_1= 797$	$Ar_1=539$	$Ar_1=573$
	$Ac_3 = 902$	$Ar_3=679$	$Ar_3=751$

From Table IV, it can be seen that the austenite start temperatures during the first heating cycle of Steel A and Steel *A1* are significantly different (~33 °C). It is well known in the case of fully ferritic or ferritic + pearlitic steels, that the austenite formation temperatures depend on the heating rate and amount and morphology of pearlite [16, 17]. Furthermore, the sensitivity of austenite formation temperature increases with heating rate [18]. However, there is less work in the literature comparing the austenite formation kinetics of ferritic and bainitic/martensitic microstructures. Furthermore, the Ar_3 temperature of the two steels during cooling after the second pass are different (~26 °C). This could indicate that composition (i.e. both the microstructure and distribution of alloying elements in the microstructure) might be different at the peak temperature of 860 °C in Steel A and Steel *A1*. The effect of these differences in phase transformation temperatures could potentially change the amount of MA constituent in the final steel microstructure. In order to test this hypothesis, characterization of the ICRHAZ microstructures from Steel A and Steel *A1* were performed.

Analysis of Optical Microstructure. Analysis of Steel A and Steel *A1* microstructures focused on the quantification of the MA constituents. The samples were etched in Le Pera's reagent [5], which clearly reveals the MA constituents as brightly imaging regions under an optical microscope. Figure 8(a) shows a typical image obtained from Steel A after etching using Le Pera's etchant. The darkly imaging regions are ferrite constituents and the mottled brightly imaging regions are MA constituents. Using image analysis techniques, Figure 8(b), the amount of MA constituent in the microstructure was estimated for both Steel A and Steel *A1*. From SEM analysis of the microstructures, Figure 9, these MA constituents ranged from 1-4 µm. These regions appear to be present at ferrite grain boundaries and in a few instances, near grain boundary triple points. Predominantly, the morphology of the MA constituents appeared to be polygonal or blocky. However, elongated (aspect ratio ranging from 1:3 to 1:5) MA constituents were also common.
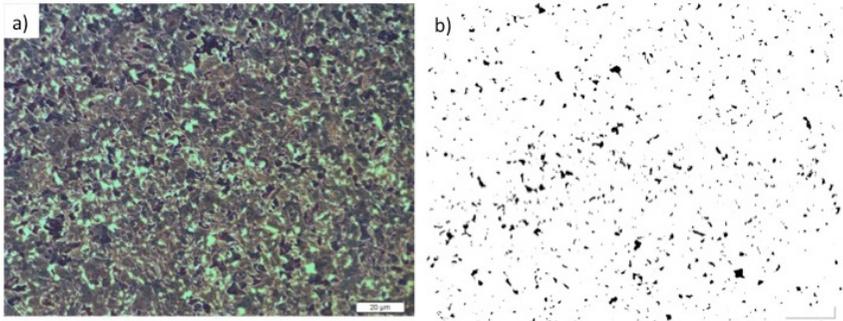
Figure 8. (a) Microstructure of Steel A after ICRHAZ thermal cycle when etched with Le Pera's etchant showing bright regions (MA constituents) and darker (ferritic) regions and (b) Image analysis of Figure 8(a); Bright MA constituents are isolated and shown as dark regions.
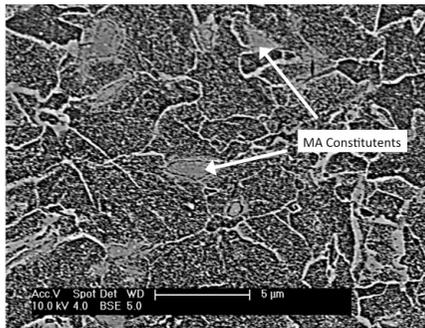

Figure 9. SEM image of ICRHAZ microstructure of Steel A showing MA constituents present at ferrite grain boundaries.

Table V shows the amount of MA constituents calculated in Steel A and Steel *A1* from image analysis of optical micrographs taken from the steels. It was found that Steel *A1*, which had an initial microstructure consisting of a mixture of bainite and martensite, showed a lower amount of MA constituents than Steel A.

Table V. Comparison of the Amount of MA Constituents Present in the ICRHAZ Region of
Steel A and Steel A1 from Analysis of Optical Images

Steel	Amount of MA constituent%
Steel A	2.9 ± 0.81
Steel *A1*	1.4 ± 0.76

The significance of these differences in MA constituents is being evaluated with toughness
(behavior under dynamic strain rate) and tensile testing (behavior under constant strain rate).
This difference in MA constituents present in two steels with different initial microstructures, but
having the same chemical composition, does suggest that the initial microstructure might also
play a vital role in governing the final properties at the HAZ of welded steels.

Analysis of Large Multi-Pass Weld HAZ

Dilatometry. In this section, the results of dilatometry analysis and of microstructure
characterization are provided for the 16 weld pass HAZ thermal simulation on Steel A and Steel
B. Figure 6 shows the 16 pass weld thermal cycle used for the thermal simulation. From the
graph it is evident that only three of the HAZ peaks (passes 8, 10 and 13) lie above 700 °C. The
highest peak temperature during the multipass weld HAZ thermal cycles was 1281 °C. The
heating rate was ~200 °C /s and the cooling rate ($t_{8/5}$) was ~18 °C /s in a Gleeble Thermo-
mechanical simulator. Table VI shows the on-heating and on-cooling transformation start and
finish temperatures for Steel A and Steel B, obtained from dilatometric analysis of those three
main peaks (passes 8, 10 and 13). It can be seen from the table that Steel B appeared to have a
slightly lower Ac_1 and Ac_3 temperature than Steel A. However, no significant differences were
measured between the Ar_1 and Ar_3 temperatures of the two steels. In order to observe the
microstructure obtained from both Steel A and Steel B after the HAZ thermal cycle,
microstructure characterization was performed as discussed below.

Table VI. On-Heating and On-Cooling Transformations of Steel A and Steel B during Multi-Pass
Weld HAZ Simulation (passes 8, 10 and 13)

Steel	On-Heating	On-Cooling
Steel A	$Ac_1 = 836 \pm 7$ °C	$Ar_1 = 655 \pm 27$ °C
	$Ac_3 = 910 \pm 13$ °C	$Ar_3 = 495 \pm 15$ °C
Steel B	$Ac_1 = 824 \pm 11$ °C	$Ar_1 = 643 \pm 16$ °C
	$Ac_3 = 898 \pm 16$ °C	$Ar_3 = 491 \pm 18$ °C

Microstructure Analysis

Figure 10(a) and 10(b) show the optical microstructure from the simulated 16 weld pass HAZ
Gleeble samples of Steel A and Steel B. Both figures show polygonal ferrite microstructures
with the grain size ranging from ~6-10 µm. Compared to the as-rolled microstructure of Steel A,
the grains of the simulated HAZ show an increase in average grain size of ~3-5 µm. In the case
of Steel B, the microstructure changed from a predominantly acicular/Widmanstätten
microstructure to one of polygonal ferrite. This effect is due to the absence of rolling strain on
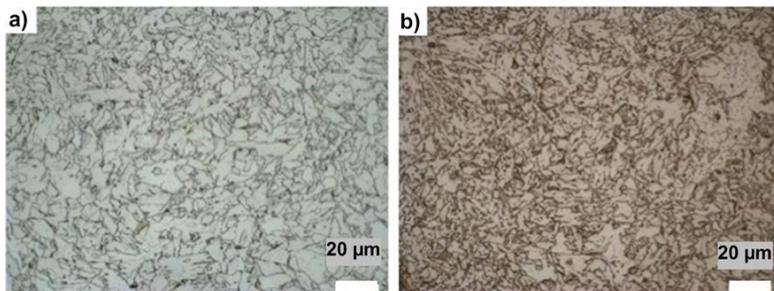transformation during welding.

Figure 10. Optical micrographs of (a) Steel A and (b) Steel B after multi-pass weld HAZ thermal cycle predominantly showing polygonal ferrite grains.
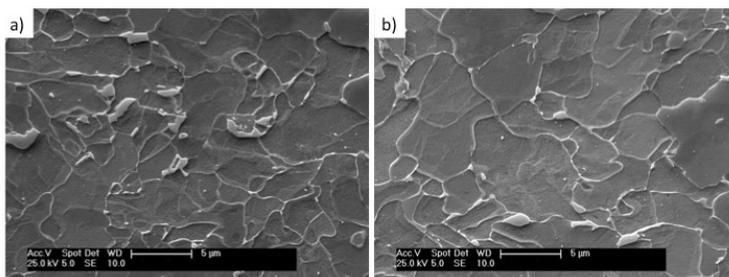

Figure 11. SEM images of microstructures of (a) Steel A and (b) Steel B after multi-pass weld HAZ thermal cycles showing polygonal ferrite grain size 6-10 µm.

Figures 11(a) and 11(b) show the SEM secondary electron image of the HAZ microstructures of Steel A and Steel B respectively. From the SEM images, it can be clearly seen that the microstructures of HAZ simulated Steel A and Steel B are very similar i.e. polygonal ferrite grains with grain size ~6-10 µm along with some second phase regions present at the ferrite grain boundaries. In order to determine the mechanical heterogeneity in the heat treated samples, micro hardness indents were made over the sample cross-sections. Thousands of indents spaced 200 µm apart were made using a load of 300 g. A color scale map was generated based on the hardness data obtained. Figure 12 shows the hardness distribution of the HAZ simulated Steel A, Figure 12(a), and Steel B, Figure 12(b). From the hardness distribution map, micro-hardness measurements over the simulated HAZ Gleeble sample cross sections ranged from 209 ± 4.8 HV and 229 ± 6.8 HV, in A and B, respectively.
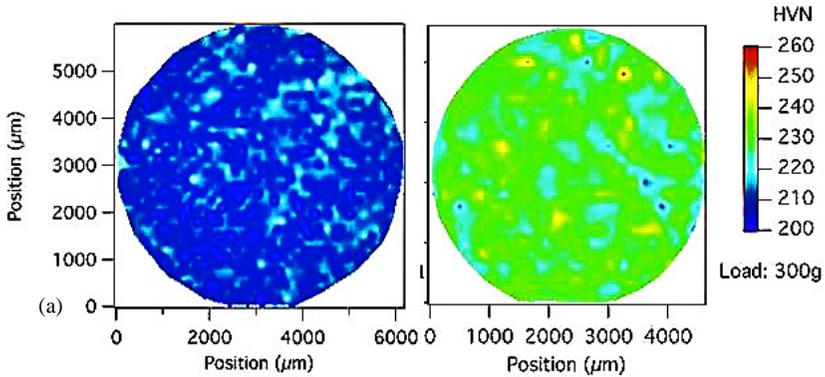
Figure 12. Hardness maps generated from the cross sections of simulated multipass weld HAZ Gleeble samples of (a) Steel A and (b) Steel B.

Even though the two steels show a difference (~20 HV) in average hardness after the multi-pass weld HAZ thermal cycle, the microstructure of the two steels appear very similar to each other. Further mechanical testing of the HAZ simulation samples is underway to evaluate the effect of the same on toughness and tensile properties. However, preliminary analysis of the microstructure of these steels after the HAZ simulation suggests that the effect of initial microstructure on the final properties and microstructure of the HAZ might not be significant if base material is subjected to a multi-pass weld heat treatment involving a large number of weld passes with varying peak temperatures.

Conclusions

In this study, two steels with different initial microstructures but the same initial composition, when subjected to an ICFGHAZ thermal cycle, showed a difference in MA constituents in the final microstructure. This difference could signify that initial microstructure might play a role in the development of the final microstructure in the HAZ (especially ICRHAZ) after welding and hence govern the HAZ properties.

This difference in the amount of MA constituent could be related to differences in reaustenitization kinetics of the different initial microstructures. However, further study is required to confirm this hypothesis. Furthermore, extensive mechanical testing is required to evaluate the significance of this difference in MA constituent.

Additionally, two steels of different compositions and different initial microstructures when subjected to a multi-pass weld thermal cycle with high peak temperatures showed similar microstructures after the HAZ simulation. This might indicate that the role of initial microstructure might not be significant if the steel is subjected to several thermal cycles involving high austenitization temperatures.

295

References

1. M.G. Akben, B. Bacroix and J.J. Jonas, "Effect of Vanadium and Molybdenum Addition on High Temperature Recovery, Recrystallization and Precipitation Behavior of Niobium-Based Microalloyed Steels," *Acta Metallurgica*, 31 (1) (1983), 161-174.

2. D.A. Porter and K.E. Easterling, *Phase Transformations in Metals and Alloys* (CRC Press, 2009).

3. S. Lee, B.C. Kim and D. Kwon, "Correlation of Microstructure and Fracture Properties in Weld Heat Affected Zones of Thermomechanically Controlled Processed Steels," *Metallurgical Transactions A*, 23A (1992), 2803-2816.

4. B.C. Kim et al., "Microstructure and Local Brittle Zone Phenomena in High-Strength Low Alloy Steel Welds," *Metallurgical and Materials Transactions A*, 22A (1991), 139-149.

5. D. Fairchild, (Ph.D. thesis, The Ohio State University, 1987).

6. C.L. Davis and J.E. King, "Cleavage Initiation in the Intercritically Reheated Coarse-Grained Heat-Affected Zone: Part I. Fractographic Evidence," *Metallurgical and Materials Transactions A,* 25A (3) (1994), 563-573.

7. K. Ohya et al., "Microstructures Relevant to Brittle Fracture Initiation at the Heat-Affected Zone of Weldment of a Low Carbon Steel," *Metallurgical and Materials Transactions A*, 27A (1996), 2574-2582.

8. J.H. Chen et al., "Micro-Fracture Behaviour Induced by MA Constituent (Island Martensite) in Simulated Welding Heat Affected Zone of HT80 High Strength Low Alloyed Steel," *Acta Metallurgica*, 32 (1984), 1779-1788.

9. C.L. Davis and J.E. King, "Effect of Cooling Rate on Intercritically Reheated Microstructure and Toughness in High Strength Low Alloy Steel," *Materials Science and Technology*, 9 (1993), 8-15.

10. Z.L. Zhou and S.H. Liu, "Influence of Local Brittle Zones on the Fracture Toughness of High-Strength Low Alloyed Multipass Weld Metals," *Acta Metallurgica Sinica*, 11 (2) (1998), 87-92.

11. Y. Li et al., "The Effect of Vanadium and Niobium on the Properties and Microstructure of the Intercritically Reheated Heat Affected Zone in Low Carbon Microalloyed Steels," *The Iron and Steel Institute of Japan International*, 41 (1) (2001), 46-55.

12. E. Bonnevie et al., "Morphological Aspects of Martensite-Austenite Constituents in Intercritical and Coarse Grain Heat Affected Zones of Structural Steels," *Materials Science and Engineering A*, 385 (2004), 352-358.

13. C.L. Davis and J.E. King, "Cleavage Initiation in the Intercritically Reheated Coarse-Grained Heat-Affected Zone: Part II. Failure Criteria and Statistical Effects," *Metallurgical and Materials Transactions A,* 27A (1996), 3019-3029.

14. H. Qiu et al., "Fracture Mechanism and Toughness of the Welding Heat-Affected Zone in Structural Steel Under Static and Dynamic Loading," *Metallurgical and Materials Transactions A*, 31A (2000), 2000-2785.

15. Eweld predictor: https://eweldpredictor.ewi.org/portal/home

16. F.G. Caballero, C. Garcia-Mateo and C.G. de Andres, "Modelling of Kinetics of Austenite Formation in Steels with Different Initial Microstructures," *The Iron and Steel Institute of Japan International*, 41 (10) (2001), 1093-1102.

17. F.G. Caballero, C. Garcia-Mateo and C.G. de Andres, "Influence of Pearlite Morphology and Heating Rate on the Kinetics of Continuously Heated Austenite Formation in Eutectoid Steel," *Metallurgical and Materials Transactions A*, 32 (2001), 1283-1291.

18. F.G. Caballero, C. Garcia-Mateo and C.G. de Andres, "Influence of Scale Parameters of Pearlite on the Kinetics of Anisothermal Pearlite-to-Austenite Transformation in Eutectoid Steel," *Scripta Materialia*, 42 (2000), 1159-1164.